Tunable random lasing in dye-doped mesoporous silica SBA-15

Fábio S. De Vicente,[1] Leandro X. Moreno,[1] Marcus V. A. Prado,[2,3] Luis M. G. Abegão,[4,5] Leandro A. Melo,[2,3] José J. Rodrigues, Jr.,[2,3] and Márcio A. R. C. Alencar[2,3,*]

[1]*Universidade Estadual Paulista (UNESP), IGCE, Departamento de Física, 13506–900, Rio Claro, SP, Brazil*
[2]*Universidade Federal de Sergipe (UFS), Departamento de Física, 49100-000, São Cristóvão, SE, Brazil*
[3]*Universidade Federal de Sergipe (UFS), Laboratório de Corrosão e Nanotecnologia (LCNT), 49100-000, São Cristóvão, SE, Brazil*
[4]*Universidade de São Paulo (USP), Instituto de Física de São Carlos, 13560–970, São Carlos, SP, Brazil*
[5]*Instituto de Física, Universidade Federal de Goiás, 74690-900, Goiânia, GO, Brazil*

(Received 23 October 2020; revised 25 January 2021; accepted 3 February 2021; published 25 February 2021)

Mesoporous silica, known as SBA-15, possesses a hexagonal pore structure, with 8-nm-diameter pores and high surface area ($\sim$700 m^2/g). The mesoporosity of SBA-15 is excellent to be filled with luminescent chromophores aiming at optical and photonic applications. SBA-15 powder infiltrated with Rhodamine B (RB) was prepared with different RB loads. Using the second harmonic of a pulsed Nd:yttrium aluminum garnet (YAG) laser (8 ns, 10 Hz) as the excitation source, the light emission spectra of the samples were investigated. Typical incoherent feedback random laser behavior was observed. Tunable random laser emissions from 579 to 585 nm were obtained depending on the excitation laser spot diameter and the RB load. The results indicate that mesoporous SBA-15 infiltrated with RB is a promising material for the development of solid-state random lasers.

DOI: 10.1103/PhysRevMaterials.5.025203

I. INTRODUCTION

Random lasing is a physical phenomenon in which efficient stimulated emission of radiation is achieved due to feedback mechanisms provided by light scattering [1,2]. This is a natural phenomenon that might occur in space [3]; however, as a device, it has been proposed by Letokhov more than 50 y ago [4] and has been observed in different natural and man-made light-scattering systems since then [1,2,5–8]. Exploiting its unique features, several applications have been proposed based onrandom lasers, such as cancer diagnostics [9,10], sensors [11], imaging [12], and time-resolved microscopy [13], among others [1,2].

Aiming at the development of efficient lighting devices, there is a huge interest in solid-state random laser (RL) systems [1,2,5,7,14–26]. In this approach, the scattering properties of porous systems [27–33] can be exploited to generate the required laser feedback mechanism, while their solid structure support organic molecules used as gain media. Among the multitude of porous materials, mesoporous silica materials known as SBA-15 present a barely exploited huge potential for the development of random lasers. This medium is synthesized via surfactant-templated sol-gel route during the hydrolysis of silicon alkoxide yielding a class of material that possesses a well-ordered hexagonal pore structure, with 8-nm-diameter cylindrical pores and high surface area ($\sim$700 m^2/g) [34]. Additionally, the cylindrical pores of SBA-15 can be changed by synthesis achieving up to 30-nm-diameter. SBA-15 mesoporous silica materials have been used for several applications and research in catalysis and purification [35,36], biosensors [37], and drug delivery [38,39].

Recently, functionalized mesoporous SBA-15 materials were applied as a fluorescent sensor for detection of heavy metals in water [40–42]. Also, Rhodamine-doped porous materials have been receiving attention due to their novel properties with potential applications in biology and medicine [43]. The mesopores of SBA-15 are excellent to be filled with luminescent chromophores aiming at optical and photonic applications [44,45], and their pore structure is interesting to produce light-scattering effects.

Previous works reported fluorescence studies of SBA-15 doped with laser dyes [44–49]. Fluorescence features of Rhodamine B incorporated in SBA-15 mesoporous silica were reported [44–46] and more recently, amplified stimulated emission in SBA-15 doped with Coumarin and DCJTB laser dyes were investigated [47–49]. In comparison with others solid-state hosts, the advantage of the use of SBA-15 as a RL material includes its simplified preparation, the possibility of shape [50], and of the pores' dimensions [51–55] tuning, allied to its high surface to volume ratio, variable framework compositions, and high thermal stability. Also, the mesoporous SBA-15 is a versatile material for anchoring a variety of molecules with optical properties aiming at random laser design. Nevertheless, several features of RL in this system, such as tunability and the effect of doping concentration on the laser emission characteristics, have not been reported yet to the best of our knowledge.

In this work we report the tunable RL effect in mesoporous SBA-15 powders infiltrated with two distinct amounts of Rhodamine B. The prepared samples were characterized by nitrogen adsorption-desorption analyses, thermogravimetric analyses (TG), scanning electron microscopy (SEM) and

*marca.ufs@gmail.com

transmission electron microscopy (TEM), luminescence, and RL emission. The RL emission was characterized by analyzing the emission spectra of the investigated samples when illuminated by a nanosecond pulsed laser, under distinct excitation conditions.

II. MATERIALS AND METHODS

A. Ordered mesoporous silica SBA-15 synthesis

Ordered mesoporous silica SBA-15 powders were prepared by hydrolysis of tetraethylorthosilicate (TEOS, Sigma-Aldrich 99%) added to an acid solution of surfactant template triblock copolymer Pluronic P123 (Sigma-Aldrich) in water. The acid solution of the surfactant template was prepared by dissolving 4.0 g of copolymer P123 in 30 ml of deionized water with subsequent addition of 120 ml of 2 M HCl under mechanical stirring maintained at 35 °C for 20 h. After, 8.5 g of TEOS was added dropwise to the P123 acid solution and the mixture was maintained under mechanical stirring at 35 °C for 24 h for complete hydrolysis. After this period the container was sealed and temperature of the mixture was maintained at 80 °C for 16 h to increase the condensation of the silica network. Decreasing the temperature of the mixture to ambient, a white powder was precipitated and the supernatant liquid was removed. The precipitated powder was dried at 80 °C for 24 h and calcined at 550 °C for 5 h in air (heating rate 2 °C/min) to complete removal of the organic P123 template. Details of the SBA-15 synthesis and characterizations are reported elsewhere [56].

B. Rhodamine B-doped SBA-15 synthesis

Rhodamine B has been infiltrated into mesoporous silica SBA-15 powders by a simple method without previous silica surface modifications. An ethanolic solution of 25 mg of Rhodamine B (Sigma-Aldrich, 99%) in 100 ml of ethanol was prepared and to this solution was added 0.3 g of SBA-15 powder in an Erlenmeyer flask. Then the flask was sealed and the mixture ultrasonicated for 30 min at room temperature.

In a second step, the mixture of SBA-15 with ethanolic solution of Rhodamine B was held under reflux and stirring at 80 °C for 24 h. After reflux and temperature decrease to ambient the samples were transferred to specific flasks and centrifuged (4000 rpm for 15 min). After centrifugation the supernatant was removed from the flasks and the decanted powder of SBA-15 doped with Rhodamine B was dried at 80 °C for 24 h. These samples were nominated SBA-RB1. The powder of SBA-15 doped with Rhodamine B (SBA-RB1) was washed again in ethanol at 80 °C for 1 h with intention of removing some Rhodamine B that was not completely infiltrated into the mesoporous sample. After this process the sample was centrifuged again (4000 rpm for 15 min), and a slightly clear SBA-15 powder doped with Rhodamine B was obtained compared with the SBA-RB1. These samples were nominated SBA-RB2.

C. Surface and thermal analysis

Analysis of surface area and porosimetry of pure and RB-doped SBA-15 powders were performed by nitrogen adsorption-desorption isotherms obtained at liquid nitrogen temperature (77 K), using Micromeritics ASAP 2010 equipment, with samples previously degassed at 120 ºC for 24 h under vacuum.

The specific surface area (S_{BET}) was determined using the Brunauer-Emmett-Teller (BET) method. The pore volume per mass unit (V_p) obtained as Barrett-Joyner-Halenda (BJH) nitrogen adsorption cumulative pore volume was calculated by the BJH method. Pore-size distribution (PSD) was determined from the adsorption isotherms using the DFT PLUS MICROMERITICS software based on the classical Kelvin equation and the Harkins and Jura isotherm model for cylindrical pores [50,57].

Thermogravimetric analysis was carried out in a synthetic air atmosphere with a heating rate of 10 °C/min, using a Shimadzu Thermal Analyzer TA-50.

D. Scanning electron microscopy

A powder sample of SBA-15 doped with Rhodamine B was prepared for scanning electron microscopy imaging. The powder was dispersed and slightly compressed onto a double-sided carbon tape mounted in a metallic stub. To improve the SEM imaging a thin layer of gold was deposited on the mounted samples. The metallization of the samples was made by using a sputtering-system model 108 Auto Sputter from Cressington. The SEM images were acquired by using a benchtop SEM, model eXpress from Aspex, operated at an acceleration voltage of 15 keV.

E. Transmission electron microscopy

A small amount of powder sample was suspended in 5 mL of ethanol by sonication. A drop of the suspension was evaporated on an ultrathin carbon film supported by a lacy carbon film on a 400-mesh cooper grid. The TEM images were recorded at CMNano-UFS using a JEOL JEM-1400 plus equipment operating at 120 kV, equipped with a charge-coupled device (CCD) camera (Gatan).

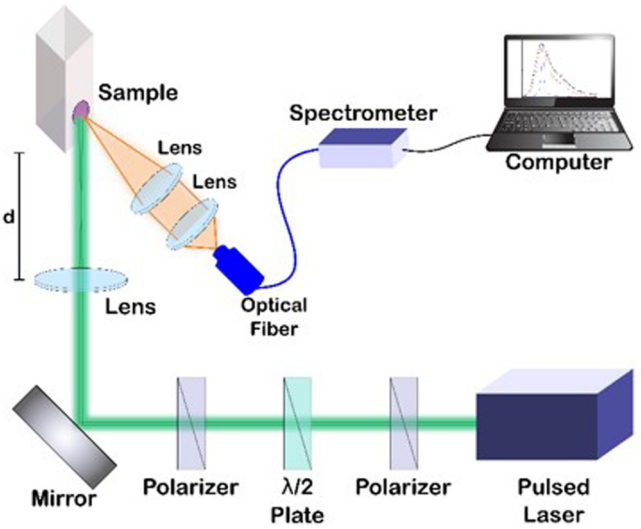

FIG. 1. Experimental setup for luminescence and random laser measurements.

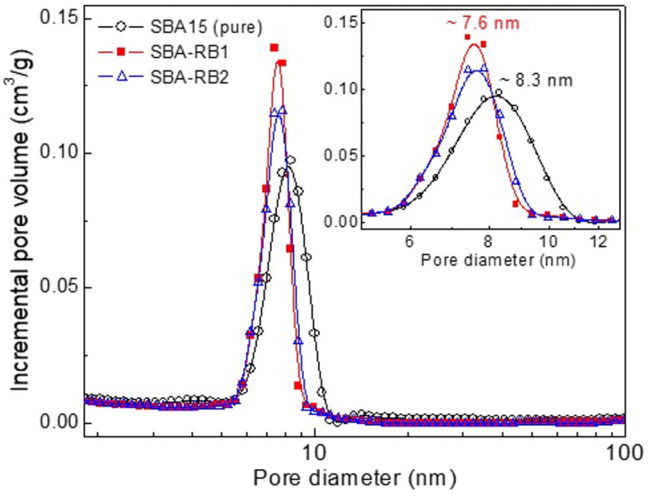

FIG. 2. Pore-size distribution of SBA-15, SBA-RB1, and SBA-RB2 powders. Inset shows details of the pore-size distribution for pure and RB-doped SBA powders.

F. Random laser investigation experiments

For luminescence experiments, the powdered samples were fixed on a glass slide using carbon tape. This slide was then placed on a sample holder in the experimental setup displayed schematically in Fig. 1. The second harmonic of a Nd:YAG pulsed laser (8-ns duration time and 10-Hz repetition rate) was used as the excitation source. The excitation power was controlled continuously by a set of half-wavelength plate and two polarizers. The laser beam was focused by a 10.0 cm convergent lens, which was placed on a translation stage that enabled us to vary the distance "d" between the sample and the lens. Using this approach, the laser spot diameter on the sample surface could be adjusted by changing the value of d. The incidence angle of the laser beam on the sample surface was about 45°. The emitted light was collected normally to the sample surface by a set of lenses and analyzed spectrally by a CCD compact spectrometer. The sample's emission spectra were measured for different excitation powers and distinct excitation spot diameters.

Analyzing the emission intensity and linewidth as a function of the excitation fluence, the random laser emission was characterized. Typically, the emission spectra of random lasers must present threshold behaviors, understood as abrupt changes on the luminescence intensity and spectral width with the pumping energy [1,2]. The threshold can be defined as the value of the excitation fluence or intensity that is associated with an inflection point of a sigmoidal fit applied to the linewidth data [58]. Furthermore, if the threshold value changes with the excitation laser spot diameter, the observed stimulated emission depends indeed on the multiple scattering process, which characterizes a random laser [1,2,20].

III. RESULTS AND DISCUSSION

A. Nitrogen adsorption

Figure 2 shows the pore-size distribution evaluated for cylindrical pores for the pure SBA-15 powder sample and for the Rhodamine B-doped SBA-15 powder samples, SBA-RB1 and SBA-RB2.

The PSD of pure SBA-15 sample shows a narrow peak at mean pore diameter of 8.33 nm, which is typical of the ordered cylindrical pores in mesoporous silica SBA-15. For the SBA-RB1 and SBA-RB2 samples the PSD peaks are slightly narrower and shifted toward smaller pore diameter around 7.60 nm. This indicates that Rhodamine B molecules were anchored inside the pore's wall, causing a decrease in its mean pore diameter. Nevertheless, the overall porosity with well-defined pore diameter was preserved for the RB-doped SBA-15 samples.

Table I summarizes the experimental values for the specific surface area S_{BET}, the mean pore diameter d_p, and the total pore volume per mass unit V_p, obtained from the nitrogen adsorption surface analysis for the pure and RB-doped samples. The position (in terms of the mean pore diameter d_p) of the PSD peaks were evaluated based on the PSD curves as described elsewhere [50].

The anchoring of organic dye molecules onto the solid mesoporous silica changes its textural properties, which influences the surface area and porosity of the samples. Pure SBA-15 sample presented surface area of 714 m^2/g and pore diameter of 8.33 nm while SBA-RB1 sample presented an increased surface area of 768 m^2/g and pore diameter of 7.57 nm. The sample SBA-RB2, with the lowest Rhodamine B content, presented surface area of 744 m^2/g and pore diameter of 7.66 nm. These results are consistent with the anchoring of Rhodamine B onto the SBA-15 matrix, causing a slight increase in its surface area, as well as a decrease in its mean pore diameter with the incorporation of the dye inside the pores of the mesoporous silica.

B. Thermal analysis

Thermogravimetric analyses were performed to determine the amount of RB incorporated in the SBA-15 powders (Fig. 3). TG analyses revealed a mass loss above 200 °C due to the decomposition of RB. The results indicate that the samples SBA-RB1 and SBA-RB2 have incorporated 7.0 and 5.0% of RB (in mass %), respectively. Due to the high reactivity of SBA-15 surface, the mass loss below 200 °C is related to moisture adsorbed.

TABLE I. Surface analysis parameters of the pure SBA-15 and RB-doped SBA-15 obtained from nitrogen adsorption isotherms.

Sample	Surface area, S_{BET} (m^2/g)	Mean pore diameter, d_p (nm)	Total pore volume, V_p (cm^3/g)
SBA-15	714 (4)	8.33 (4)	0.795 (5)
SBA-RB1	768 (4)	7.57 (4)	0.820 (4)
SBA-RB2	744 (4)	7.66 (3)	0.797 (4)

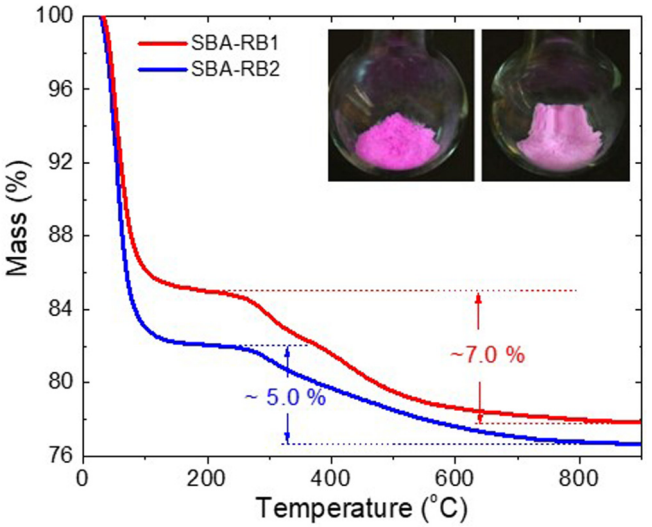

FIG. 3. Thermogravimetric analyses of SBA-15 powders doped with two different RB dye concentrations. The inset shows a photography of the samples SBA-RB1 (left) and SBA-RB2 (right) with different loads of RB.

C. Scanning electron microscopy

The produced powders exhibit nonuniform size and shape distributions, as can be seen in the SEM images shown in Fig. 4. The samples consisted of fiber-shaped micrometric-sized particles with porous structure. Due to this morphology, these powders are excellent hosts for anchoring a large number of dye molecules and can exhibit efficient light scattering. These are essential properties for suitable solid-state random laser materials.

D. Transmission electron microscopy

Figure 5 presents a typical TEM image of the produced mesoporous particles. Despite the micrometric nonuniform shape and size distribution visualized on SEM images, a closer look revealed that, in nanoscale, the particles consist of ordered set of channels less than 10 nm wide, which is in good agreement with the nitrogen adsorption's results.

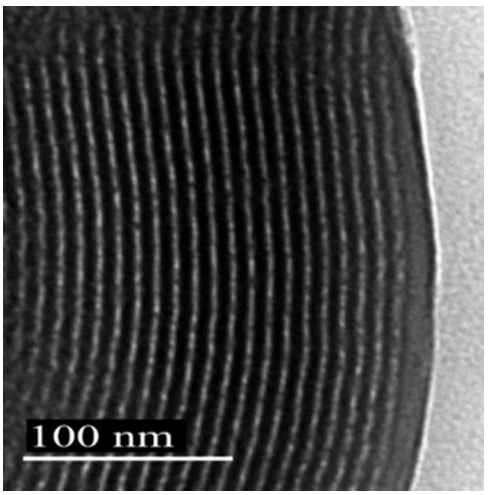

FIG. 5. TEM image of the SBA-15 powder particle.

E. Luminescence and random laser characterizations

Figure 6 presents the normalized fluorescence spectra of SBA-RB1 and SBA-RB2 samples, excited by a laser beam with 0.5 μJ/mm^2 fluence of the second harmonic of a Nd:YAG pulsed laser. As can be observed, RB-doped SBA-15 samples presented typical fluorescence spectra of Rhodamine B when excited with low pump power. In this case, the fluorescence spectra showed two characteristic broad Gaussian bands, one more intense at nearly 575 nm (related to monomers of RB) and another less intense band at 625 nm related to dimers of RB. Moreover, it can also be observed that both spectra of SBA-RB1 and SBA-RB2 are slightly shifted due to differences in RB concentrations incorporated in the samples. Indeed, the spectrum of the sample with larger amount of incorporated dye (SBA-RB1) presents a redshift of approximately 3.5 nm in comparison with the lower dye con-

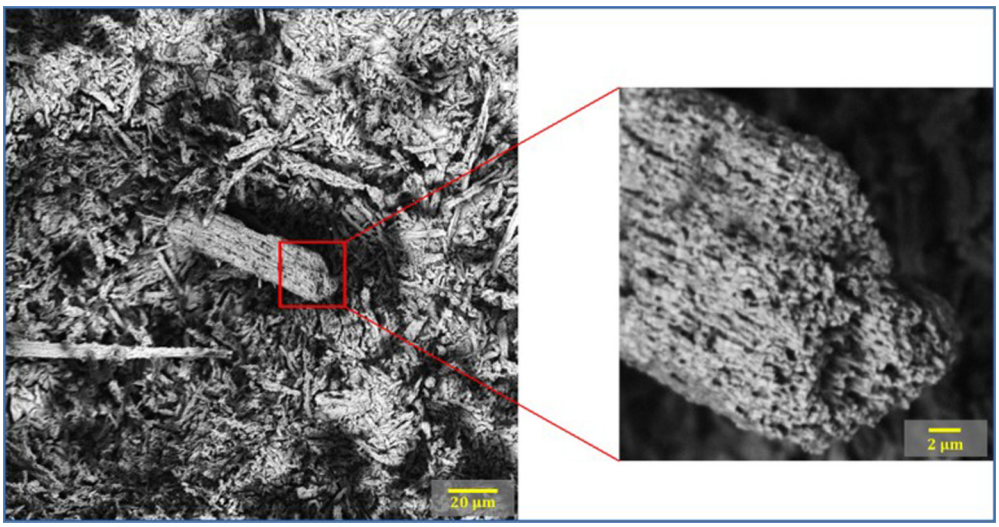

FIG. 4. SEM images of the SBA-15 powder.

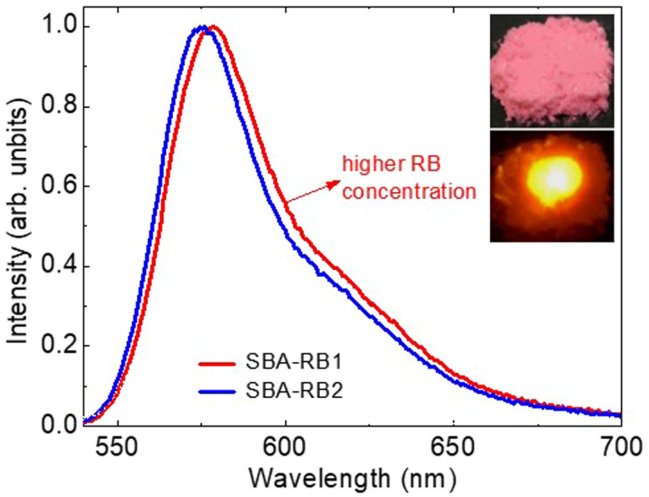

FIG. 6. Emission spectra of SBA-RB1 and SBA-RB2 samples at low pump fluence of excitation (0.5 μJ/mm^2, 532 nm, 8 ns). The inset shows a photograph of the SBA-RB1 powder under ambient light (top) and under excitation of a 405-nm laser spot (down).

centration sample (SBA-RB2). This behavior was observed previously [59] and can be attributed to a larger contribution of dimers to the observed luminescence of the sample with the highest amount of dye molecules.

In Fig. 7 the RL emission spectra measured as a function of the pump fluence are presented. By increasing the pump laser fluence, the emission spectra of both samples presented nonlinear increases on the peak intensity as well as significant linewidth narrowing, as shown in Figs. 7(a) and 7(b). At high excitation fluence [Fig. 7(c)], both samples presented smooth redshifted and much narrower emission spectra (full width at half maximum ∼7.0 nm) in comparison to that observed for samples under low excitation fluence. Again, samples with the higher load of RB (SBA-RB1) presented a spectrum slightly shifted to lower energies, when compared with the spectrum of the SBA-RB2 sample. In this excitation configuration, the emission of SBA-RB2 presented a maximum intensity at 582 nm, while the emission peak of SBA-RB1 sample was observed at 584 nm. Although the peak wavelengths indicate that the observed luminescence is dominated by the monomers emission [20,53], the redshift under higher excitation power suggests that reabsorption processes due to monomers and dimers might be contributing to the observed narrow-linewidth emission.

These results suggest that both samples present typical RL emission with nonresonant feedback [1,2]. Nevertheless, the determination of the emission threshold and its dependence on the excitation volume are required to be verified if this is indeed the observed. Hence, we analyzed the emission intensity and linewidth as a function of the pump fluence.

Figure 8 shows the behavior of the emission peak intensity and linewidth as a function of the excitation fluence. The RL threshold was obtained following van Soest definition as the inflection point of a sigmoidal fit through the linewidth curve [52]. As can be observed in this figure, both samples presented the typical threshold behavior for excitation with a 1.9-mm laser spot diameter. The peak intensity presented the characteristic nonlinear growth as the pump fluence was raised, as shown in Figs. 8(a) and 8(b). It was also observed that both samples exhibited a strong linewidth reduction when the excitation fluence was increased. For SBA-RB1, the linewidth was reduced from 42.0 to 7.3 nm, while a linewidth reduction from 40.1 to 7.0 nm was observed for SBA-RB2. For both samples, the RL threshold was equal to 5×10^2 mJ/mm^2, as indicated in Figs. 8(c) and 8(d).

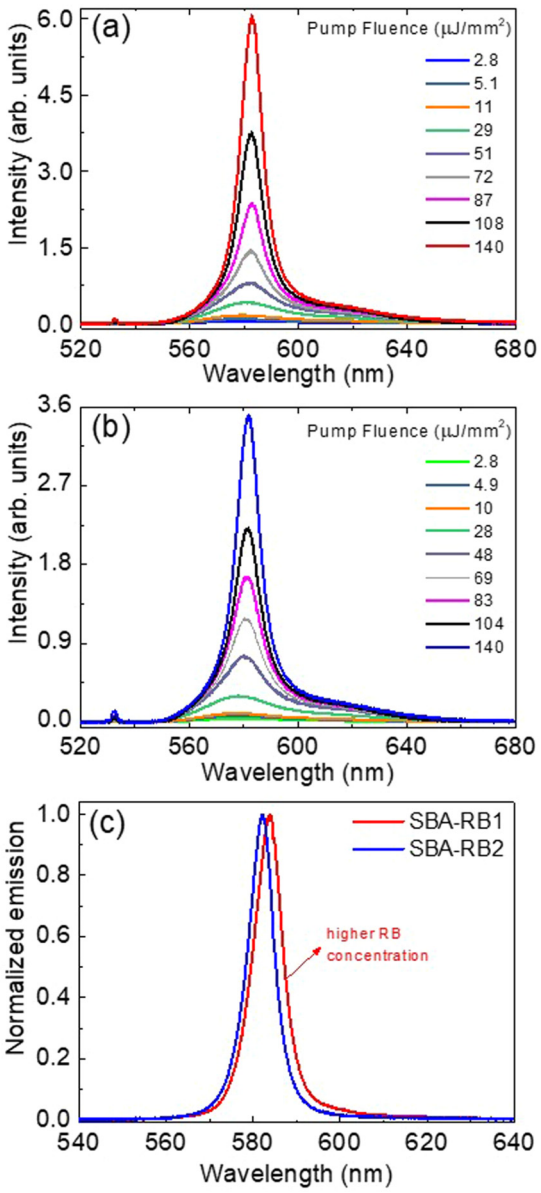

FIG. 7. RL emission spectra evolution as a function of the pump fluence. Laser excitation spot diameter equal to 1.9 mm: (a) SBA-RB1 and (b) SBA-RB2. (c) Normalized emission of both samples excited with 0.95 mJ/mm^2.

The experiment was repeated for different excitation laser spot diameters. The same behavior was observed at all experimental conditions exploited. However, as shown in Fig. 9, we verified for both samples that the threshold values were reduced as the excitation spot diameter was raised. Moreover, the higher the amount of dye, the lower is the threshold for

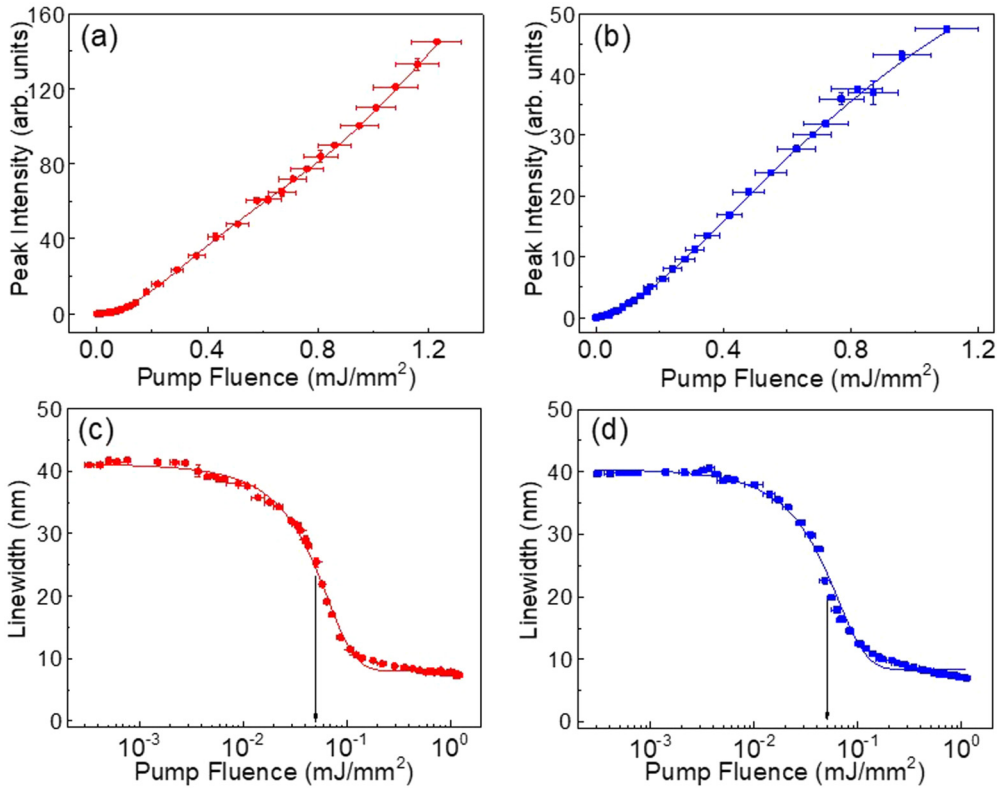

FIG. 8. Emission peak intensity vs pump fluence for SBA-RB1 (a) and SBA-RB2 (b). Emission linewidth vs pump fluence for SBA-RB1 (c) and SBA-RB2 (d). The solid lines are guides to the eyes. Excitation spot diameter equal to 1.9 mm.

excitation spot diameter smaller than 1.0 mm. This dependence of the threshold value on the excitation spot diameter and gain medium concentration confirms that the observed emission is scattering dependent. This result characterizes this phenomenon as random laser with incoherent feedback [20].

It is worth mentioning that different spectral shifts of the emitted RL peak were observed for distinct excitation conditions and for the samples with different dye concentrations. In this experiment excitation spot diameters of 0.33 mm up to 1.92 mm were used with fixed pump fluence of 0.75 mJ/mm^2.

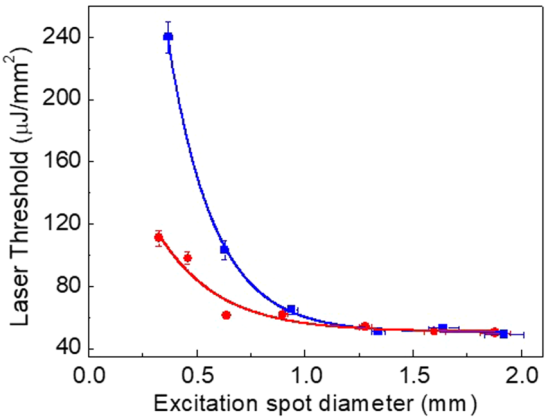

FIG. 9. RL threshold as a function of excitation spot diameter for SBA-RB1 (solid red circles) and SBA-RB2 (solid blue squares). The solid lines are guides to the eyes.

These results are summarized in Fig. 10(a). Also, the pump fluence was varied from 0.65 up to 1.00 mJ/mm^2 for each spot diameter and the same behavior was observed.

In all investigated excitation configurations, sample SBA-RB1 presented emission peaks redshifted in comparison with the correspondent measured spectra for SBA-RB2. For both samples, the RL emission peaks redshift with the increase of the excitation spot diameter from 0.3 to 1.25 mm, as presented in Fig. 10(a). This can be understood as evidence of the reabsorption process due to the presence of dye monomers. On the other hand, for excitation spot diameters larger than 1.25 mm the spectral shift presents a reverse behavior (blueshift). This suggests that another absorption channel, due to the presence of dimers within the samples, is also contributing to the spectral shift of the emitted RL.

The different emission peak values observed at distinct excitation conditions suggests that a certain degree of tuning control can be achieved using this dye-doped mesoporous powder material, similarly as observed in colloidal systems [60]. As in those experiments, the spectral shift obtained here by varying the excitation area relies on the scattering feedback. The light is more strongly amplified in larger active volumes, as demonstrated by Fig. 9, which in turn enhances the reabsorption effects. Therefore, this is indeed a distinct result from the amplified spontaneous emission phenomenon, which does not depend on light-scattering processes [20,52], previously reported on SBA-15 doped with different organic dyes [47–49]. As already mentioned, previous works have investigated the luminescence from dye-doped ordered [44–49] and disordered [19,27–33] porous systems. However,

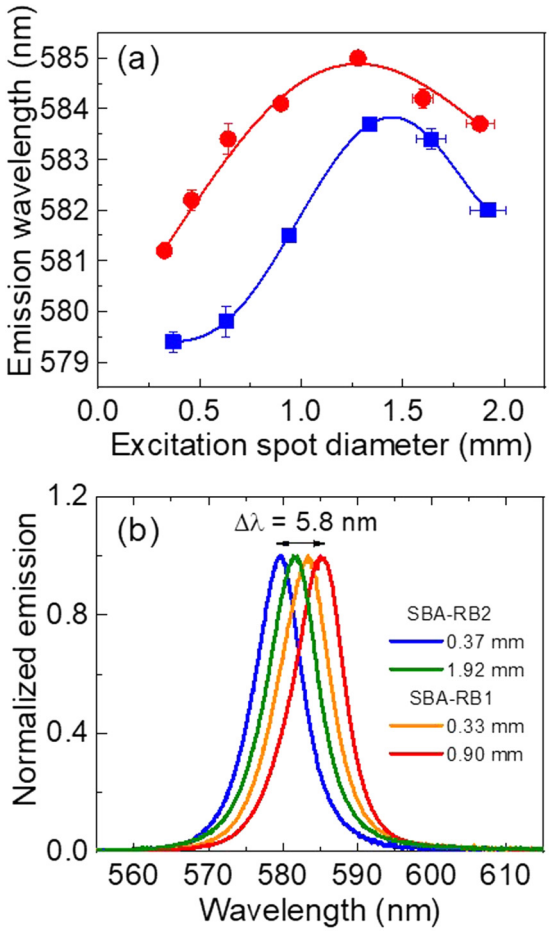

FIG. 10. (a) Emission wavelength as a function of excitation spot diameter for SBA-RB1 (solid red circles) and SBA-RB2 (solid blue squares) samples. The solid lines are guides to the eyes. (b) Selected normalized emission spectra of both samples (SBA-RB1 and SBA-RB2) for distinct excitation spot diameters.

here emission from dye-doped SBA-15 mesoporous silica is characterized as RL. In addition, the amount of dye of the powdered samples was accurately measured and its influence on the RL characteristics was evaluated.

Combining dye molecules concentration and the excitation spot diameter, the RL wavelength could be tuned from 579.5 to 585.3 nm [Fig. 10(b)]. Such results demonstrate that the wavelength of the random laser emission from this porous system can be controlled. Owing to the nanosized diameter of the pores, we believe light scattering on the irregular surfaces of the powder particles gives the main contribution to the nonresonant feedback mechanism of the observed emission. Nevertheless, the mesoporous structure of the SBA-15 is essential to enable the tunability of these systems. This ∼5.8 nm emission wavelength variation was possible with a small change on the rhodamine amount (only 2% in mass), associated with a reduction of the pore diameter. Indeed, due to the pores, the available surface area in which the dye could be attached to the silica is increased in comparison with solid particles of the same size. Hence, in porous systems, the number of organic molecules attached to the particles can be varied within a much larger range than it would be possible in solid particles counterparts. As the number of dimers is directly related to the dye molecules concentration and the redshift of the emission is associated with the monomers and dimers reabsorption processes, a suitable choice of dye concentration and excitation conditions might generate even wider tunability range for solid-state random lasers based on this kind of hybrid system.

Due to the wide range of applications that can be developed exploiting the chemical and physical properties of mesoporous silica, its use as a RL host can improve even further the SBA-15 application potential, in which the laser emission can act as a luminescent probe or sensor, providing additional functionalities to this hybrid system. For instance, it is well known that mesoporous silica SBA-15 is a material that shows potential characteristics for use in nanomedicine as a vaccine vehicle for humans [61] and as a nanocarrier for drug delivery [39,62,63]. Hence, combining the random laser emission to the host properties, the system formed by SBA-15 and Rhodamine B can be exploited as an excellent carrier to be delivered into *in vivo* tissue [64], as well as a promising material for biocompatible RL fluorescence probe for *in vivo* imaging and diagnosis [10]. Moreover, owing to the possibility of wavelength tuning displayed by the Rhodamine B doped SBA-15, this system can also be employed as random laser source for full-field optical coherence tomography [65,66] and speckle-free laser imaging [12], among other RL applications.

IV. CONCLUSION

In summary, incoherent feedback random laser emission was observed from Rhodamine B-doped SBA-15 powdered systems. Nonuniform micrometer-sized particles with an internal mesoporous structure were synthesized. Two samples with a distinct concentration of dye were prepared, and their emission spectra characterized. A slight redshift on the emission spectrum was observed for the sample with the highest dye concentration, which could be interpreted as a consequence of an increase on the amount of dye aggregates within the sample. Exploiting this feature, it was possible to control the RL emission wavelength of this hybrid material. Indeed, by combining the excitation spot diameter and the samples dye concentration, the random laser emission peak wavelength could be tuned over a range of ∼6 nm. Our results demonstrate the huge potential the mesoporous systems exhibit for the development of tunable solid-state random lasers.

ACKNOWLEDGMENTS

Financial support from CNPQ (Conselho Nacional de Desenvolvimento Científico e Tecnológico), FAPESP/SP (Fundação de Amparo à Pesquisa do Estado de São Paulo), and FAPITEC/SE (Fundação de Apoio à Pesquisa e à Inovação Tecnológica do Estado de Sergipe) are acknowledged. This work was financed in part by the Coordenação de Aperfeiçoamento de Pessoal de Nível Superior (CAPES, Brasil) and was performed in the framework of the National Institute of Photonics (INCT de Fotônica), Grant No. 465763/2014-6, MCTI/CNPq/FACEPE.

[1] D. S. Wiersma, The physics and applications of random lasers, Nat. Phys. **4**, 359 (2008).

[2] F. Luan, B. Gu, A. S. L. Gomes, K.-T. Yong, S. Wen, and P. N. Prasad, Lasing in nanocomposite random media, Nano Today **10**, 168 (2015).

[3] V. Letokhov and S. Johansson, *Astrophysical Lasers* (Oxford University Press, Oxford, 2008).

[4] V. S. Letokhov, Generation of light by a scattering medium with negative resonance absorption, JETP **26**, 835 (1968).

[5] M. A. Noginov, *Solid-State Random Lasers* (Springer-Verlag, New York, 2005).

[6] N. M. Lawandy, R. M. Balachandran, A. S. L. Gomes, and E. Sauvain, Laser action in strongly scattering media, Nature (London) **368**, 436 (1994).

[7] A. Costela, L. Cerdán, and I. García-Moreno, Solid state dye lasers with scattering feedback, Prog. Quantum Electron. **37**, 348 (2013).

[8] W. Guerin, N. Mercadier, F. Michaud, D. Brivio, L. S. Froufe-Pérez, R. Carminati, V. Eremeev, A. Goetschy, S. E. Skipetrov, and R. Kaiser, Towards a random laser with cold atoms, J. Opt. **12**, 024002 (2010).

[9] R. C. Polson and Z. V. Vardeny, Random lasing in human tissues, Appl. Phys. Lett. **85**, 1289 (2004).

[10] Y. Wang, Z. Duan, Z. Qiu, P. Zhang, J. Wu, D. Zhang, and T. Xiang, Random lasing in human tissues embedded with organic dyes for cancer diagnosis, Sci. Rep. **7**, 8385 (2017).

[11] L. M. G. Abegão, A. A. C. Pagani, S. C. Zílio, M. A. R. C. Alencar, and J. J. Rodrigues, Measuring milk fat content by random laser emission, Sci. Rep. **6**, 35119 (2016).

[12] B. Redding, M. A. Choma, and H. Cao, Speckle-free laser imaging using random laser illumination, Nat. Photonics **6**, 355 (2012).

[13] A. Mermillod-Blondin, H. Mentzel, and A. Rosenfeld, Time-resolved microscopy with random lasers, Opt. Lett. **38**, 4112 (2013).

[14] H. Cao, Y. G. Zhao, S. T. Ho, E. W. Seelig, Q. H. Wang, and R. P. H. Chang, Random Laser Action in Semiconductor Powder, Phys. Rev. Lett. **82**, 2278 (1999).

[15] L. Long, D. He, W. Bao, M. Feng, P. Zhang, D. Zhang, and S. Chen, Localized surface plasmon resonance improved lasing performance of Ag nanoparticles/organic dye random laser, J. Alloys Compd. **693**, 876 (2017).

[16] R. M. Balachandran, D. P. Pacheco, and N. M. Lawandy, Laser action in polymeric gain media containing scattering particles, Appl. Opt. **35**, 640 (1996).

[17] S. K. Turitsyn, S. A. Babin, A. E. El-Taher, P. Harper, D. V. Churkin, S. I. Kablukov, J. D. Ania-Castãón, V. Karalekas, and E. V. Podivilov, Random distributed feedback fibre laser, Nat. Photonics **4**, 231 (2010).

[18] M. A. S. de Oliveira, C. B. de Araújo, and Y. Messaddeq, Upconversion ultraviolet random lasing in Nd^{3+} doped fluoroindate glass powder, Opt. Express **19**, 5620 (2011).

[19] R. Barbosa-Silva, A. F. Silva, A. M. Brito-Silva, and C. B. de Araújo, Bichromatic random laser from a powder of rhodamine-doped sub-micrometer silica particles, J. Appl. Phys. **115**, 043515 (2014).

[20] L. M. G. Abegão, D. S. Manoel, A. J. G. Otuka, P. H. D. Ferreira, D. R. Vollet, D. A. Donatti, L. De Boni, C. R. Mendonça, F. S. De Vicente, J. J. Rodrigues *et al.*, Random laser emission from a Rhodamine B-doped GPTS/TEOS-derived organic/silica monolithic xerogel, Laser Phys. Lett. **14**, 065801 (2017).

[21] S. Gottardo, R. Sapienza, P. D. García, A. Blanco, D. S. Wiersma, and C. López, Resonance-driven random lasing, Nat. Photonics **2**, 429 (2008).

[22] N. B. Tomazio, L. F. Sciuti, G. F. B. de Almeida, L. De Boni, and C. R. Mendonca, Solid-state random microlasers fabricated via femtosecond laser writing, Sci. Rep. **8**, 13561 (2018).

[23] M. Montinaro, V. Resta, A. Camposeo, M. Moffa, G. Morello, L. Persano, K. Kazlauskas, S. Jursenas, A. Tomkeviciene, J. V. Grazulevicius *et al.*, Diverse regimes of mode intensity correlation in nanofiber random lasers through nanoparticle doping, ACS Photonics **5**, 1026 (2018).

[24] Y. Liu and X. Meng, Enabling random lasing in an ultrabroad spectral range with robust platforms based on amorphous media, Nanoscale **10**, 17275 (2018).

[25] Y. J. Lee, T. W. Yeh, Z. P. Yang, Y. C. Yao, C. Y. Chang, M. T. Tsai, and J. K. Sheu, A curvature-tunable random laser, Nanoscale **11**, 3534 (2019).

[26] X. Li, F. Hong, S. Wang, S. He, S. Jin, J. Guo, H. Yuan, Q. Lv, S. Hu, P. Wang *et al.* A tunable blue random laser based on solid waveguide gain films with plasmonics and scatters, J. Alloys Compd. **790**, 558 (2019).

[27] S. Murai, K. Fujita, J. Konishi, K. Hirao, and K. Tanaka, Random lasing from localized modes in strongly scattering systems consisting of macroporous titania monoliths infiltrated with dye solution, Appl. Phys. Lett. **97**, 031118 (2010).

[28] S. J. Marinho, L. M. Jesus, L. B. Barbosa, D. Reyes Ardila, M. A. R. C. Alencar, and J. J. Rodrigues, Bi-chromatic random laser from alumina porous ceramic infiltrated with rhodamine B, Laser Phys. Lett. **12**, 055801 (2015).

[29] H.-W. Shin, S. Y. Cho, K.-H. Choi, S.-L. Oh, and Y.-R. Kim, Directional random lasing in dye-TiO_2 doped polymer nanowire array embedded in porous alumina membrane, Appl. Phys. Lett. **88**, 263112 (2006).

[30] J. Lü, T. Fan, and G. Chen, Random laser action in dye doped nanoporous polymeric film, Opt. Commun. **356**, 17 (2015).

[31] I. Viola, N. Ghofraniha, A. Zacheo, V. Arima, C. Conti, and G. Gigli, Random laser emission from a paper-based device, J. Mater. Chem. C **1**, 8128 (2013).

[32] Y. Wang, X. Shi, Y. Sun, R. Zheng, S. Wei, J. Shi, Z. Wang, and D. Liu, Cascade-pumped random lasers with coherent emission formed by Ag–Au porous nanowires, Opt. Lett. **39**, 5 (2014).

[33] M. V. Santos, É. Pecoraro, S. H. Santagneli, A. L. Moura, M. Cavicchioli, V. Jerez, L. A. Rocha, L. F. C. de Oliveira, A. S. L. Gomes, C. B. de Araújo *et al.*, Silk fibroin as a biotemplate for hierarchical porous silica monoliths for random laser applications, J. Mater. Chem. C **6**, 2712 (2018).

[34] D. Zhao, J. Feng, Q. Huo, N. Melosh, G. H. Fredrickson, B. F. Chmelka, and G. D. Stucky, Triblock copolymer syntheses of mesoporous silica with periodic 50 to 300 angstrom pores, Science **279**, 548 (1998).

[35] X. Wang, K. S. K. Lin, J. C. C. Chan, and S. Cheng, Direct synthesis and catalytic applications of ordered large pore aminopropyl-functionalized SBA-15 mesoporous materials, J. Phys. Chem. B **109**, 1763 (2005).

[36] Y. Yang, J. Li, G. Lv, and L. Zhang, Novel method to synthesize Ni_2P/SBA-15 adsorbents for the adsorptive desulfurization of model diesel fuel, J. Alloys Compd. **745**, 467 (2018).

[37] A. Mirabi, A. S. Rad, Z. Khanjari, and M. Moradian, Preparation of SBA-15/graphene oxide nanocomposites for preconcentration and determination of trace amounts of rutoside in blood plasma and urine, Sens. Actuators, B **253**, 533 (2017).

[38] V. Nairi, L. Medda, M. Monduzzi, and A. Salis, Adsorption and release of ampicillin antibiotic from ordered mesoporous silica, J. Colloid Interface Sci. **497**, 217 (2017).

[39] V. Fathi Vavsari, G. Mohammadi Ziarani, and A. Badiei, The role of SBA-15 in drug delivery, RSC Adv. **5**, 91686 (2015).

[40] N. Lashgari, A. Badiei, and G. Mohammadi Ziarani, A novel functionalized nanoporous SBA-15 as a selective fluorescent sensor for the detection of multianalytes (Fe^{3+} and $Cr_2O_7^{2-}$) in water, J. Phys. Chem. Solids **103**, 238 (2017).

[41] L. Zhao, D. Sui, and Y. Wang, Fluorescence chemosensors based on functionalized SBA-15 for detection of Pb^{2+} in aqueous media, RSC Adv. **5**, 16611 (2015).

[42] X. Wang, P. Wang, Z. Dong, Z. Dong, Z. Ma, J. Jiang, R. Li, and J. Ma, Highly sensitive fluorescence probe based on functional SBA-15 for selective detection of Hg^{2+}, Nanoscale Res. Lett. **5**, 1468 (2010).

[43] B. Martins Estevão, I. Miletto, L. Marchese, and E. Gianotti, Optimized Rhodamine B labeled mesoporous silica nanoparticles as fluorescent scaffolds for the immobilization of photosensitizers: A theranostic platform for optical imaging and photodynamic therapy, Phys. Chem. Chem. Phys. **18**, 9042 (2016).

[44] Q. He, J. Shi, X. Cui, J. Zhao, Y. Chen, and J. Zhou, Rhodamine B-co-condensed spherical SBA-15 nanoparticles: Facile co-condensation synthesis and excellent fluorescence features, J. Mater. Chem. **19**, 3395 (2009).

[45] M. Guli, Y. Chen, X. Li, G. Zhu, and S. Qiu, Fluorescence of postgrafting Rhodamine B in the mesopores of rodlike SBA-15, J. Lumin. **126**, 723 (2007).

[46] J. Tu, N. Li, Y. Chi, S. Qu, C. Wang, Q. Yuan, X. Li, and S. Qiu, The study of photoluminescence properties of Rhodamine B encapsulated in mesoporous silica, Mater. Chem. Phys. **118**, 273 (2009).

[47] D. Zhang, S. Zhang, D. Ma, and X. Li, Low threshold amplified spontaneous emission based on coumarin 151 encapsulated in mesoporous SBA-15, Appl. Phys. Lett. **89**, 231112 (2006).

[48] D. Zhang, Z. Duan, Y. Wang, P. Zhang, and S. Chen, Amplified spontaneous emission from DCJTB encapsulated in mesostructured composite silica SBA-15, Appl. Opt. **55**, 4736 (2016).

[49] M. Guli, X. Li, K. Zhang, and Y. Chi, Photoluminescence and laser properties of mesostructured SBA-15 monolith doped with coumarin 151, J. Sol-Gel Sci. Technol. **54**, 329 (2010).

[50] A. Katiyar, S. Yadav, P. G. Smirniotis, and N. G. Pinto, Synthesis of ordered large pore SBA-15 spherical particles for adsorption of biomolecules, J. Chromatogr. A **1122**, 13 (2006).

[51] A. Roucher, A. Bentaleb, E. Laurichesse, M.-A. Dourges, M. Emo, V. Schmitt, J.-L. Blin, and R. Backov, First MACRO-MESOCELLULAR Silica SBA-15-Si(HIPE) monoliths: Conditions for obtaining self-standing materials, Chem. Mater. **30**, 864 (2018).

[52] F. Wu, G. Ye, Y. Liu, R. Yi, X. Huo, Y. Lu, and J. Chen, New short-channel SBA-15 mesoporous silicas functionalized with polyazamacrocyclic ligands for selective capturing of palladium ions in HNO_3 media, RSC Adv. **6**, 66537 (2016).

[53] B. Ma, L. Zhuang, and S. Chen, Rapid synthesis of tunable-structured short-pore SBA-15 and its application on CO2 capture. J. Porous Mater. **23**, 529 (2016).

[54] Y. Wang, F. Zhang, Y. Wang, J. Ren, C. Li, X. Liu, Yun Guo, Y. Guo, and G. Lu, Synthesis of length controllable mesoporous SBA-15 rods, Mater. Chem. Phys., **115** (2–3), 649 (2009).

[55] M. Kruk and L. Cao, Pore size tailoring in large-pore SBA-15 silica synthesized in the presence of hexane, Langmuir **23**, 7247 (2007).

[56] T. da Silveira, C. M. Awano, D. A. Donatti, F. S. de Vicente, and D. R. Vollet, About the thermal stability and pore elimination in the ordered hexagonal mesoporous silica SBA-15, Microporous Mesoporous Mater. **190**, 227 (2014).

[57] S. J. Gregg and K. S. W. Sing, *Adsorption, Surface Area, and Porosity* (Academic Press, New York, 1967).

[58] G. van Soest, M. Tomita, and A. Lagendijk, Amplifying volume in scattering media, Opt. Lett. **24**, 306 (1999).

[59] A. Lewkowicz, A. Synak, B. Grobelna, L. Kułak, and P. Bojarski, Spectroscopic properties of Rhodamine B entrapped in hybrid porous nanolayers at high dye concentration, Chem. Phys. **439**, 121 (2014).

[60] M. A. F. de Souza, A. Lencina, and P. Vaveliuk, Controlling bichromatic emission in scattering gain media, Opt. Lett. **31**, 1244 (2006).

[61] K. Scaramuzzi, G. D. Tanaka, F. Mariano Neto, P. R. A. F. Garcia, J. J. M. Gabrili, D. C. A. Oliveira, D. V. Tambourgi, J. S. Mussalem, D. Paixão-Cavalcante, M. T. D'Azeredo Orlando, V. F. Botosso, C. L. P. Oliveira, M. C. A. Fantini, and O. A. Sant'Anna, Nanostructured SBA-15 silica: An effective protective vehicle to oral hepatitis B vaccine immunization, Nanomed. Nanotechnol. Biol. Med., **12**, 2241 (2016).

[62] S.-W. Song, K. Hidajat, and S. Kawi, Functionalized SBA-15 materials as carriers for controlled drug delivery: influence of surface properties on matrix−drug interactions, Langmuir **21**, 9568 (2005).

[63] M. K. Rasmussen, H. N. Bordallo, M. A. Bordenalli, M. A. Akamatsu, A. G. Trezena, M. Tino-De-Franco, O. A. Sant'Anna, T. da Silva Martins, J. L. de Souza Lopes, M. C. de Abreu Fantini, and C. L. Pinto Oliveira, Assessing the efficiency of SBA-15 as a nanocarrier for diphtheria anatoxin, Microporous Mesoporous Mater. **312**, 110763 (2021).

[64] E. Ignesti, F. Tommasi, L. Fini, F. Martelli, N. Azzali, and S. Cavalieri, A new class of optical sensors: A random laser based device, Sci. Rep. **6**, 35225 (2016).

[65] B. Redding, M. A. Choma, and H. Cao, Spatially incoherent random lasers for full field optical coherence tomography, in *CLEO:2011 - Laser Applications to Photonic Applications, OSA Technical Digest (CD)* (Optical Society of America, 2011), paper PDPC7.

[66] H. Cao, B. Redding, and M. A. Choma, U.S. Patent No. US20140111671A1 (2012).